ACS APPLIED MATERIALS & INTERFACES

Research Article

www.acsami.org

Ambient Synthesis of High-Quality Ruthenium Nanowires and the Morphology-Dependent Electrocatalytic Performance of Platinum-Decorated Ruthenium Nanowires and Nanoparticles in the Methanol Oxidation Reaction

Christopher Koenigsmann,[†] Dara Bobb Semple,[†] Eli Sutter,[‡] Sybil E. Tobierre,[§] and Stanislaus S. Wong*[,†,§]

[†]Department of Chemistry, State University of New York at Stony Brook, Stony Brook, New York 11794-3400, United States

[‡]Center for Functional Nanomaterials, Brookhaven National Laboratory, Building 735, Upton, New York 11973, United States

[§]Condensed Matter Physics and Materials Sciences Department, Brookhaven National Laboratory, Building 480, Upton, New York 11973, United States

Supporting Information

ABSTRACT: We report for the first time (a) the synthesis of elemental ruthenium nanowires (Ru NWs), (b) a method for modifying their surfaces with platinum (Pt), and (c) the morphology-dependent methanol oxidation reaction (MOR) performance of high-quality Pt-modified Ru NW electrocatalysts. The synthesis of our elemental Ru NWs has been accomplished utilizing a template-based method under ambient conditions. As-prepared Ru NWs are crystalline and elementally pure, maintain electrochemical properties analogous to elemental Ru, and can be generated with average diameters ranging from 44 to 280 nm. We rationally examine the morphology-dependent performance of the Ru NWs by comparison with commercial Ru nanoparticle (NP)/carbon (C) systems after decorating the surfaces of these structures with Pt. We have demonstrated that the deposition of Pt onto the Ru NWs (Pt∼Ru NWs) results in a unique hierarchical structure, wherein the deposited Pt exists as discrete clusters on the surface. By contrast, we find that the Pt-decorated commercial Ru NP/C (Pt∼Ru NP/C) results in the formation of an alloy-type NP. The Pt∼Ru NPs (0.61 A/mg of Pt) possess nearly 2-fold higher Pt mass activity than analogous Pt∼Ru NW electrocatalysts (0.36 A/mg of Pt). On the basis of a long-term durability test, it is apparent that both catalysts undergo significant declines in performance, potentially resulting from aggregation and ripening in the case of Pt∼Ru NP/C and the effects of catalyst poisoning in the Pt∼Ru NWs. At the conclusion of the test, both catalysts maintain comparable performance, despite a slightly enhanced performance in Pt∼Ru NP/C. In addition, the measured mass-normalized MOR activity of the Pt∼Ru NWs (0.36 A/mg of Pt) was significantly enhanced as compared with supported elemental Pt (Pt NP/C, 0.09 A/mg of Pt) and alloy-type PtRu (PtRu NP/C, 0.24 A/mg of Pt) NPs, both serving as commercial standards.

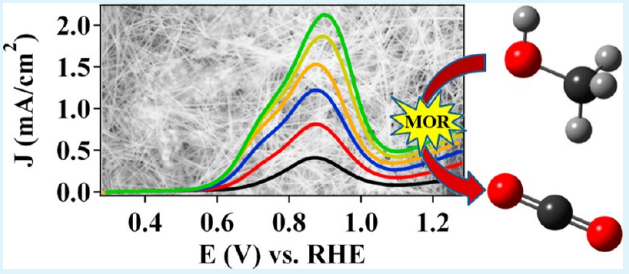

KEYWORDS: *direct methanol fuel cells, electrocatalysis, one-dimensional nanostructures, noble metals, template-based synthesis, morphology-dependent behavior*

1. INTRODUCTION

Recently, nanostructured ruthenium (Ru) metal and ruthenium oxide (RuO_2) have been the focus of considerable attention, particularly in their application as heterogeneous catalysts.[1−3] By comparison with other noble metals, such as platinum (Pt) for instance, Ru is significantly less costly and more abundant, while also maintaining high conductivity, good thermal stability, and relatively high corrosion resistance.[4] In addition, nanoparticulate Ru has been successfully employed as a catalyst for a variety of industrially relevant reactions including the Fischer−Tropsch process,[5] the re-formation of natural gas,[6] the carbon monoxide (CO) oxidation reaction,[7] and many more.[1,3] Others have also demonstrated the growth of epitaxial graphene layers on Ru(0001) single crystals, which possess exciting applications in electronics, sensing, and catalysis.[8]

More broadly, nanostructured Ru has also become a ubiquitous component of anode catalysts in direct methanol fuel cells (DMFCs).[9−12] Although elemental Pt is traditionally considered to be the most active noble metal for the oxygen reduction reaction (ORR), commercial carbon-supported platinum nanoparticles (Pt NP/C) maintain low activities toward the methanol oxidation reaction (MOR) because of their susceptibility to CO poisoning at potentials relevant for

Received: February 27, 2013
Accepted: May 20, 2013
Published: June 6, 2013

   dx.doi.org/10.1021/am4007462 | ACS Appl. Mater. Interfaces 2013, 5, 5518−5530

effective DMFC operation (e.g., 0.1−0.5 V).[13−16] A key step toward overcoming the issue of CO poisoning on Pt catalysts has been to introduce measurable amounts of Ru into Pt, thereby forming bimetallic, alloy-type NPs.[9,17] These commercially available $Pt_{1-x}Ru_x$ alloy-type particles ($Pt_{1-x}Ru_x$ NP/C) are believed to follow a so-called "bifunctional mechanism", wherein oxidation of the primary poisoning intermediate CO is facilitated by the more oxophilic Ru sites. The Ru sites adsorb oxygen species (e.g., $Ru-OH_{ads}$) at lower potentials than Pt and preferentially oxidize adsorbed CO in a process known as carbonyl spillover.[18−20] This proposed mechanism is distinctive from the one observed on elemental Pt, wherein adsorption of oxygen species and the corresponding oxidation of CO are delayed to higher potentials. Typically, the addition of up to 30% Ru in the PtRu alloy can reduce the overpotential of MOR by more than 100 mV, thereby greatly improving the intrinsic efficiency of functional DMFCs.[9]

Although alloy-type $Pt_{1-x}Ru_x$-based MOR catalysts have shown great promise, the widespread development of these zero-dimensional (0D) electrocatalysts has been hindered by their poor durability and high Pt loading requirements.[10,21,22] A recent and interesting approach has been to adopt a more sophisticated hierarchical structure, wherein Pt is directly deposited onto the surfaces of elemental Ru nanostructures.[23−28] Inherently, this architecture localizes essentially the entire Pt content at the catalytic interface, thereby maximizing its potential catalytic efficacy and minimizing the overall quantity of Pt needed, while relegating the less expensive and more abundant Ru to the core of the material. For example, Adzic and co-workers[27] have decorated commercial carbon-supported ruthenium nanoparticles (Ru NP/C) with monolayer quantities of Pt atoms, resulting in a Pt shell−Ru NP/C core motif (e.g., Pt∼Ru NP/C). The resulting heterostructures maintained a surface area-normalized or so-called specific MOR activity that was comparable with that of commercial $Pt_{1-x}Ru_x$ alloy-type NPs (x = 0.5; PtRu NP/C). The mass-normalized activity, however, demonstrated a nearly 3-fold enhancement in the core−shell-type nanostructure over the alloy-type particle. Collectively, these results highlighted the fact that the core−shell-type architecture promotes the same bifunctional effect associated with interfacial Pt−Ru pair sites, inherent to an alloy-type NP, while requiring significantly lower levels of Pt.

In addition to tailoring the spatial distribution of Pt and Ru, significant enhancements have also been achieved by rationally tailoring the morphology of nanostructured electrocatalysts.[29−32] Specifically, one-dimensional (1D) structures, such as nanowires (NWs) and nanotubes, have been promoted as an exciting new structural paradigm for electrocatalysis by our group and several others.[31−34] 1D architectures possess several inherent advantages, such as the preferential exposure of smooth, low-energy crystalline planes, lower defect site densities, and beneficial size-dependent electronic properties, thereby collectively rendering them more active and durable toward oxygen reduction and alcohol electroxidation.[35−41] For example, our group determined that ultrathin 1D Pt NWs maintained a desirable morphology-dependent enhancement in terms of the ethanol oxidation performance, as compared with analogous commercial Pt NP/C, as a result of their unique anisotropic structure.[40] The recent progress toward the reliable synthesis and rational investigation of transition-metal-based 1D electrocatalysts has been extensively reviewed by our group.[31,32]

Although considerable improvements in activity and durability have been garnered by 1D electrocatalysts, there have been no reports, to the best of our knowledge, involving the synthesis, characterization, and electrocatalytic properties of either 1D Ru NWs or Pt-modified Ru NWs. In fact, only one report has demonstrated the synthesis of Ru NWs, utilizing electrochemical deposition, which typically involves the use of complex and expensive equipment (e.g., physical vapor deposition) and caustic reaction media and which may be potentially challenging in terms of large-scale production.[42] Accordingly, herein we report three novel advances in the development of effective and practical core−shell electrocatalysts. Specifically, first, we have tailored an ambient synthetic protocol for the production of elemental Ru NWs without requiring either surfactants, catalytic seeds, or electrochemical equipment. Second, we have rationally investigated the role of morphology upon the corresponding deposition of Pt at the catalytic interface by means of an underpotential deposition methodology followed by a galvanic displacement (UPD/GD) step; this Pt deposition protocol has been analyzed by utilizing a broad range of characterization techniques. Third, we have correlated the distinctive structure of the Pt∼Ru interface in Pt∼Ru NW and NP systems with its intrinsic electrocatalytic performance toward MOR.

The synthesis of our elemental Ru NWs has been accomplished under ambient conditions without the need for either surfactant or catalytic seeds and relies upon a proven template-based synthetic approach, developed by our group.[33,34] Our synthetic approach is advantageous, especially when it is compared with traditional electrochemical deposition techniques. Specifically, high-quality crystalline NWs can be reproducibly formed in a pH-neutral aqueous solvent, without requiring either costly electrochemical or physical vapor deposition equipment. Although the inherently low production yield associated with template-based techniques has been a key challenge, our recent efforts have demonstrated that, in certain cases, this methodology can be readily and easily scaled up to produce multigram-scale quantities of NWs.[43] Notwithstanding, our as-prepared Ru NWs are crystalline and elementally pure and can be generated with diameters ranging from 44 to 280 nm, a development that represents a crucial step toward practically incorporating 1D nanostructures for applications as varied as catalysis and nanoelectronics, for instance.

In terms of the electrocatalytic performance, electrochemical characterization, including cyclic voltammetry (CV) and CO stripping voltammetry, confirms that our as-prepared Ru NWs possess properties consistent with elemental Ru, thereby further highlighting their intrinsic quality and purity. The UPD of copper (Cu) followed by its GD[44] has been employed as a reliable method for decorating the surfaces of the Ru NWs with Pt, thereby leading to a core−shell-type structure (e.g., Pt∼Ru NWs). To rationally investigate the morphology-dependent performance in this unique hierarchical structure, we utilized the same protocol to decorate the surfaces of commercial Ru NP/C with Pt so as to form Pt∼Ru NP/C, in order to correlate the structure of the core−shell interface with the corresponding measured MOR activity. Interestingly, a thorough analysis of our as-prepared heterostructures after Pt deposition on the Ru NWs and NPs using a suite of characterization techniques reveals that Pt is not necessarily deposited as a nearly homogeneous monolayer, as had been previously suggested by Adzic and co-workers.[23] In fact, we have observed that, in particular, deposition of Pt on the Ru

NWs can result in a unique hierarchical structure, wherein the deposited Pt exists as discrete, isolated, and disparate three-dimensional (3D) clusters on the surface.

In the context of the morphology-dependent performance of the core−shell structures, we have noticed that the Pt∼Ru NPs (0.61 A/mg of Pt) possess nearly 2-fold higher activity than their analogous Pt∼Ru NW electrocatalytic counterparts (0.36 A/mg of Pt). To validate the relatively high degree of performance in the Pt∼Ru NWs, we also compared the measured mass-normalized MOR activities of the Pt∼Ru NWs (0.36 A/mg of Pt) with that of state-of-the-art, commercial Pt NP/C (0.09 A/mg of Pt) and with that of $Pt_{1-x}Ru_x$ (x = 0.5; PtRu NP/C) alloy-type NPs (0.24 A/mg of Pt). The significant and measurable enhancements observed demonstrate that our as-prepared Pt∼Ru NWs maintain a high degree of performance, especially as compared with traditional, commercial 0D catalyst architectures, but are not as promising as those of the corresponding Pt∼Ru NPs.

In addition, we have demonstrated over the entire duration of an extended durability test that the performance of both catalysts rapidly decreases and that the initial enhancement of 2-fold in the Pt∼Ru NP/C with respect to the Pt∼Ru NWs is reduced to an improvement of only 15% after the durability test. It is evident from the durability test that the considerable activity losses in the Pt∼Ru NP/C can be attributed to aggregation and ripening of the particles, whereas in the Pt∼Ru NW system, the hierarchical structure is maintained. Hence, the decline in the activity of the Pt∼Ru NWs can therefore be attributed to a poisoning effect, because fewer bimetallic Pt−Ru sites are available to catalyze the oxidation of CO and other poisoning intermediates. Collectively, the durability testing highlights both the advantages and disadvantages associated with the unique and distinctive morphologies and structures of the Pt∼Ru NW and Pt∼Ru NP/C catalysts.

2. MATERIALS AND METHODS

2.1. Synthesis of Elemental Ru NWs. The synthesis of our Ru NWs has been accomplished utilizing the ambient U-tube double-diffusion method developed by our group, and this protocol has been described in detail elsewhere.[33,36,38,41] Initially, a saturated precursor solution, consisting of 25 mM potassium hexachlororuthenate (K_2RuCl_6; Alfa Aesar, 99.95%), was prepared by dissolving the appropriate amount of solid powder (98 mg) into 10 mL of distilled water. A reducing agent solution consisting of 50 mM sodium borohydride ($NaBH_4$; Alfa Aesar, 98%) was also generated by dissolving the $NaBH_4$ powder (19 mg) in 10 mL of distilled water. Prior to assembling the U-tube, a commercially available polycarbonate (PC) membrane (Whatman, Nucleopore Track Etched), serving as the growth template, was immersed in distilled water and sonicated in order to saturate the pores. The reaction was carried out by securing the PC membrane between the two glass half-cells of the U-tube device, and subsequently the precursor and reducing agent solutions are simultaneously added to the two half-cells separated by the template.

The precursor and reducing agent solution diffuse into the template pores and react, leading to the nucleation and growth of the NW within the 1D pore channels of the membrane. Fully-formed, crystalline Ru NWs can be achieved after a reaction time of 60 min. Ru NWs with average diameters of 44 ± 4, 131 ± 14, and 280 ± 20 nm (Figure S1 in the Supporting Information, SI) could be reproducibly prepared from templates with nominal corresponding pore sizes of 15, 50, and 200 nm, respectively. The apparent discrepancy between the measured wire diameter and the nominal pore size from whence the wire was generated has been widely observed and has been discussed in detail in prior reports.[36]

Our as-synthesized Ru NWs have been isolated by first abrading the excess metallic Ru layer present on the external surfaces of the PC membrane utilizing an Arkansas Wet Stone, with mineral oil serving as a lubricant. Individual NWs have been isolated by immersing the membrane into dichloromethane (DCM) in order to fully dissolve the PC, and subsequently the mixture is centrifuged so as to separate the NWs from the DCM/PC solution. The NWs are further purified of residual organic impurities by sequentially repeating the immersion and centrifugation steps, several times. Finally, the NW powder is dispersed into a solvent, such as DCM, for further characterization and electrochemical experiments. Alternatively, free-standing NW arrays of noble metal NWs can be prepared by affixing the template onto a solid substrate (e.g., glass or silicon wafers) and exposing the substrate-supported membrane to oxygen plasma (March Plasma Etcher) for a period of 20 min.[36,38]

2.2. Structural Characterization. Powder X-ray diffraction (XRD) patterns were obtained on a Scintag powder diffractometer, operating in the Bragg−Brentano configuration using Cu Kα radiation with a scan rate of 0.25° in 2θ/min. The morphology of as-prepared Ru NWs was characterized by scanning electron microscopy (SEM) on a Leo 1550 scanning electron microscope with an operating voltage of 15 kV. Overview transmission electron microscopy (TEM) images were obtained with a Technai12 BioTwinG^2 TEM instrument equipped with an AMT XR-60 CCD camera system. High-resolution TEM (HRTEM) images, high-angle annular dark-field (HAADF) images, and energy-dispersive X-ray spectroscopy (EDAX) including both EDAX spectra and spatially resolved EDAX mapping in scanning TEM mode (STEM) as well as selected-area electron diffraction (SAED) patterns were collected on a JEOL 2100F instrument, equipped with a Gatan HAADF detector for performing incoherent HAADF or Z-contrast imaging in STEM mode at an accelerating voltage of 200 kV.

2.3. Electrochemical Characterization and Pt Deposition. Electrochemical characterization of the individual isolated Ru NWs was performed with the Ru NWs supported on a glassy carbon electrode (GCE; 5 mm, Pine Instruments). Initially, the electrode was polished to a mirror finish, using an aluminum oxide powder slurry (0.050 μm particle size). Prior to deposition of the Ru NWs, the GCE surface was premodified with a thin layer of Vulcan XC-72R carbon in order to serve as a 3D carbon support structure for the as-prepared Ru NWs.[36−38] The Ru NWs were then loaded onto the premodified GCE by adding two 5 μL drops of the Ru NW dispersion onto the surface, which was subsequently allowed to dry in air. The addition of a thin carbon layer to the GCE surface has been previously demonstrated to be useful in approximating the textured C surfaces within practical functional devices and can also contribute to an improved distribution of NWs over the geometric area of the electrode.[36,38] However, the addition of C to the electrode is not really necessary to promote a uniform distribution of the individual isolated NWs, because homogeneous dispersions of NWs can be achieved directly on the GCE surface itself.[36]

The Ru NW loaded GCE was then immersed into fresh aliquots of ethanol and water, so as to remove any impurities, prior to electrochemical characterization. Commercial Pt NP/C, commercial Ru NP/C, and commercial alloy-type $Pt_{1-x}Ru_x$ (x = 0.5; PtRu) NPs, each maintaining a 20% precious metal content (ETek), were rendered into catalyst ink dispersions (1 mg/mL) in 25% isopropyl alcohol in water and deposited directly onto the surface of polished GCE for characterization. Electrochemical measurements were obtained in either 0.1 M perchloric acid or 0.5 M sulfuric acid (Fisher Scientific, Optima grade), prepared in high-purity water with a resistivity of 18.2 MΩ cm^{-1}. Custom-made glass electrochemical cells were cleaned of residual impurities by immersing them in concentrated sulfuric acid for a period of 24 h and subsequently treating them with steam for a period of 2 h.[45] Separate electrochemical cells were employed for experiments involving perchloric and sulfuric acid electrolytes, so as to prevent contamination of perchloric acid with sulfate anions. Pt foil and an Ag/AgCl combination (3 M Cl$^-$) served as the counter and reference electrodes, respectively. All potentials have been reported with respect to the reversible hydrogen electrode.

The electrochemical properties of the Ru NWs and NPs were examined by CV and CO stripping voltammetry. Cyclic voltammograms were obtained in the desired argon-saturated electrolyte at a scan rate of 20 mV/s. The adsorption of a monolayer of CO was accomplished by immersing the electrodes into a CO-saturated electrolyte for a period of 30 min. Subsequently, the electrode was transferred to a deoxygenated electrolyte solution, so as to obtain the CO stripping voltammogram. In both cases, the electrochemically addressable surface area (ESA) of the Ru electrocatalyst was determined using the Cu UPD charge as opposed to the hydrogen adsorption (H_{ads}) charge, because the interaction of Ru−H_{ads} is weaker than that in the case of Pt and, moreover, reduction of the surface oxide adsorbates coincides with that of H_{ads}. Both of these factors mutually complicate the interpretation of the measured H_{ads} charge, in the case of Ru.[46]

Pt deposition onto the surface of the Ru NWs and commercial Ru NP was accomplished by a two-step procedure, previously employed by Adzic and co-workers[23] and by our group.[31,32] The process consists of, first, depositing a monolayer quantity of Cu ad-atoms by UPD to the surface of the Ru nanostructure and, second, initiating the GD of the Cu atoms by a Pt precursor.[44] The deposition of Cu is performed in a 50 mM $CuSO_4$ solution, prepared using 0.10 M H_2SO_4 as the supporting electrolyte. Subsequently, the Cu-modified electrode is transferred to a solution of 1.0 mM K_2PtCl_4 prepared in 50 mM H_2SO_4 under the protection of a high-purity argon atmosphere, so as to protect the Cu layer from oxidation. To ensure that the GD reaction by the Pt precursor is confined to the Cu ad-atoms and not to the Ru NW itself, we immersed the Ru NWs and Ru NPs directly (without Cu UPD) into a solution of up to 10 mM K_2PtCl_4 in either H_2SO_4 or HCl for a period of 1 h. Subsequent characterization by CV of these nanostructures, however, indicated that there is an absence of features, consistent with Pt addition, and, moreover, that there is no significant activity toward MOR.

In this case, the mass of Pt deposited was determined from the Cu UPD stripping charge of a CV curve obtained, immediately prior to deposition. Utilizing the Cu stripping charge as opposed to the deposition charge allows for calculation of the ESA without the contribution of the reduction of adsorbed surface oxide species that coincides with the UPD process in the cathodic sweep. Determination of the surface area in Ru-based catalysts has recently been investigated systematically, and the use of the Cu UPD stripping charge has been successfully utilized in our work for providing an accurate estimate of the ESA and mass of the Pt deposited at the catalyst interface.[23,27,46]

2.4. Measurement of the MOR Kinetics and Electrocatalyst Durability. The MOR kinetics were measured by first obtaining cyclic voltammograms at a scan rate of 20 mV/s in a deoxygenated solution of 0.5 M methanol (Fisher Scientific, Optima grade) supported in 0.1 M $HClO_4$, unless otherwise noted. Typically, a linear-sweep voltammogram (LSV) was obtained in the anodic sweep direction, so as to measure the MOR kinetics curves. The measured current was normalized to either the ESA or the Pt mass, which can both be determined from the Cu UPD stripping charge. After the initial LSV, the current profile of the MOR cyclic voltammogram was allowed to stabilize over the course of the first 10 complete cycles, so as to ensure that the initial current response in the LSV was reproducible. It is critical to highlight that some decline in activity was noted during the initial cycling, which was not incorporated into the subsequent durability testing. However, all electrodes in this manuscript have been tested under identical conditions, thereby rendering the possibility of a self-consistent comparison among all of the electrodes before subsequent durability testing.

After the initial decline in activity, the extended durability of the catalyst was subsequently examined by repeatedly cycling the electrode in a solution of 0.5 M methanol/0.1 M $HClO_4$ at a rate of 50 mV/s between the potentials of 0.5 and 0.9 V, so as to bracket the potential window relevant for MOR. This trend in the anodic current density has been employed as a measure of the observed behavior of the electrocatalyst over the course of 2000 electrochemical cycles. Although some activity was lost within the first 10 cycles, the purpose of the durability test utilized herein has been to explore the performance of the catalysts after extensive cycling, so as to determine the effects of poisoning and catalyst reconstruction upon the corresponding electrocatalytic performance.

The activity of our novel Pt∼Ru NWs has been compared with respect to that of Pt NP/C and PtRu NP/C (Etek and BASF), serving as commercial standards. Although a broad range of highly active commercial standards exist, these commercial catalysts have been widely employed in the literature as useful standards for analyzing and understanding the performance.[29−32] It is important to note that care must be taken during comparison of the results obtained herein to other prior data in the literature, on the basis of the quality and performance of the commercial standards utilized. Notwithstanding, we also have carefully evaluated the structure, activity, and performance of our novel core−shell NWs as compared with state-of-the-art, core−shell-type Pt∼Ru NP/C, prepared analogously as an internal standard in terms of properly benchmarking the activity and performance.

3. RESULTS AND DISCUSSION

3.1. Ambient Synthesis and Characterization of High-Quality Ru NWs. In this report, the synthesis of high-quality, crystalline Ru NWs has been achieved utilizing a simple, ambient, template-based method. Specifically, crystalline NWs are generated by the reduction of a water-soluble Ru precursor (i.e., K_2RuCl_6) by a dilute solution of sodium borohydride within the pores of a PC membrane. The nucleation and growth of the metallic Ru occur within the spatial confined regions of the anisotropic 1D pore spaces of the membrane itself, thereby leading to the potential for generating highly anisotropic nanostructures. The electroless growth of metallic Ru is particularly advantageous by comparison with traditional electrodeposition, because Ru NWs with high aspect ratios can be produced in aqueous media, without requiring the use of either caustic electrolytes or the complex physical vapor deposition equipment necessary to deposit the conductive layer onto the outer surface of the membranous template.

In terms of the spectrum of techniques that have been utilized for the production of 1D noble metal nanostructures, the U-tube methodology is particularly advantageous, because it circumvents the need for either electrochemically undesirable surfactants or catalytic seeds, which require extensive postprocessing techniques for their removal prior to their use in electrocatalysis.[33,34] Although the production yield is limited by the pore sizes and surface areas of the template utilized, this methodology represents an important advance in the synthesis of 1D structures with applications in catalysis, because high-quality NWs can be produced with direct and predictable control over the diameter, chemical composition, surface texture, and crystallinity. Thus, this methodology represents a positive and significant innovation in terms of exploring the intrinsic structural and catalytic properties of 1D nanostructures and correlating their physicochemical properties with their performance.[33]

In a more practical context, the development of a flexible template-based approach allows for the diameters of these as-prepared Ru NWs to be reliably and reproducibly controlled by the appropriate variation of the diameters of the template pores used in the synthesis. In fact, in independent runs, we have been able to generate Ru NWs with monodisperse diameters of 44 ± 4, 131 ± 14, and 280 ± 20 nm, respectively, spanning both the nanoscale and submicrometer size ranges. Furthermore, the possibility of obtaining NWs with high aspect ratios of up to 26 ± 4, in the case of the 44 nm NWs, has been demonstrated by overview SEM images in Figure S1 in the SI.

Indeed, the ability to rationally tailor the diameters of the NWs without compromising either structural quality or chemical purity is significant and can be advantageous for preparing Ru NWs with potential applications in catalysis, supercapacitance, and nanoelectronics.

The structure, purity, and crystallinity of isolated Ru NWs with a diameter of 44 nm were characterized utilizing XRD, SEM, and TEM analyses. Powder XRD (Figure S2 in the SI) data obtained from a collection of Ru NWs confirm that the NWs are composed of crystalline Ru, with no other apparent crystalline impurity phases present. Interestingly, the SEM image (Figure 1A) of an individual NW reveals that the surfaces

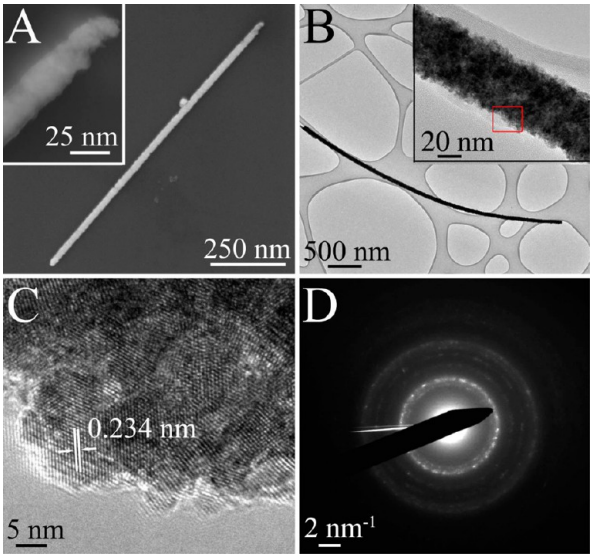

Figure 1. Overview SEM (A) and TEM (B) images of individual isolated Ru NWs. Higher-magnification SEM and TEM images are shown as insets. HRTEM (C) and SAED (D) patterns were obtained from a representative area of a central region of a typical wire, as designated by the red box.

are faceted and that the facet sizes are limited by and effectively defined by the roughened, uneven texture of the interior pore walls of the PC membranes.[15,18,19] The irregular surface texture is also apparent in Figure 1B, which provides an overview TEM image of an individual isolated NW. The TEM images in Figure 1B,C also reveal that the as-produced NWs are dense and uniform, but it is also apparent that they are composed of multiple, crystalline grains.

The HRTEM image (Figure 1C) in combination with the SAED pattern (Figure 1D) obtained from a representative region of the NW suggests that the NW is essentially polycrystalline. Inspection of the HRTEM image indicates that the well-resolved equidistant lattice planes possess an interplanar spacing of 0.234 nm, which is consistent with that of elemental Ru (0.2343 nm). The discrete diffraction rings present maintain *d* spacings that are in agreement with those observed for bulk Ru. However, a slight enlargement of the *d* spacings has been noted. This observation may result from factors, such as strain, that are highly dependent upon the morphology of the material itself. Nonetheless, our collected SAED data do not imply the formation of any rings, consistent with RuO_2, thereby confirming that only crystalline elemental Ru is present within the sample. Collectively, the XRD, SAED, and HRTEM results substantiate that our as-prepared NWs consist of essentially pure elemental Ru alone, without the presence of any other impurities.

3.2. Morphology-Dependent Electrochemical Properties of Ru NWs and Commercial Ru NP/C. The electrochemical properties of our as-prepared Ru NWs were studied to further verify their quality and purity. Indeed, the CV data (Figure 2A) obtained in 0.1 M $HClO_4$ highlight several prominent features associated with reversible surface oxidation as well as with hydrogen adsorption and desorption (H_{ads}). Herein, we observe in the cathodic segment a single broad oxide reduction feature centered at 0.43 V, which is overlaid with a second sharper reduction peak localized at 0.07 V. The reduction of the surface oxide in the cathodic sweep of Ru single crystals is a complex process and is believed to occur over multiple steps involving the initial reduction of Ru−O_{ads} to Ru−OH_{ads}, which is followed by the subsequent reduction of the Ru−OH_{ads} species itself, coinciding with the formation of Ru−H_{ads}.[47−49]

Although it is difficult to directly assign these peaks, these two reduction features are consistent with analogous results obtained on single crystals. Specifically, the first peak (0.43 V) corresponds to the reduction of surface oxides, i.e., likely Ru−O_{ads} to Ru−OH_{ads}, and the second peak (0.07 V) correlates with the combined reduction of surface oxides as well as with the UPD of the H_{ads} layer (i.e., Ru−OH_{ads} to Ru−H_{ads}). The measured reduction charge of the second peak at 0.07 V is nearly 2-fold higher than the corresponding anodic charge of the peak traditionally associated with hydrogen desorption. This finding suggests that this reduction procedure involves both the reduction of adsorbed surface oxide species as well as the H_{ads} process. The same general features are also present in the CV data obtained from the commercial Ru NP/C as compared with Ru NWs, shown in Figure 2C. However, there is one noteworthy difference. Specifically, it is apparent that the H_{ads} peaks are measurably suppressed in the Ru NP/C system, particularly in the case of the hydrogen desorption peak, suggesting that there is a weaker interaction with adsorbates in the case of the Ru NP/C catalyst.

Interestingly, the weakened interactions with adsorbates observed for Ru NP/C is also apparent in the CO stripping voltammograms (Figure 2B,D). The Ru NP/C possessed a CO stripping peak potential of 0.56 V, which was approximately 100 mV lower than that of the Ru NWs (0.68 V). It is important to highlight that the CO stripping profile garnered from Ru NP/C is consistent with prior results from other commercial Ru NP/C samples, further suggesting that there is a distinctive and real difference between the electrochemical behavior of commercial Ru NP/C catalysts versus that of our as-prepared Ru NWs.

In prior reports, our group has observed a significant diameter-dependent decrease in the CO stripping peak potential as the diameters of the wires were decreased into the nanoscale region.[31,32,36,37] This observation has been widely ascribed to a size-dependent decrease in the weighted center of the *d* band in noble metal NWs, such as Pt and Pd, as the diameter of NWs is purposely decreased to the nanoscale. For instance, the ultrathin Pt NWs were found to maintain a 200 mV lower CO stripping potential as compared with that observed for commercial Pt NP/C.[39,40] Yet, the CO stripping trend observed herein contrasts with these prior results. Indeed, the suppressed H_{ads} and enhanced CO stripping kinetics in the Ru NP/C can potentially be attributed to the residual presence

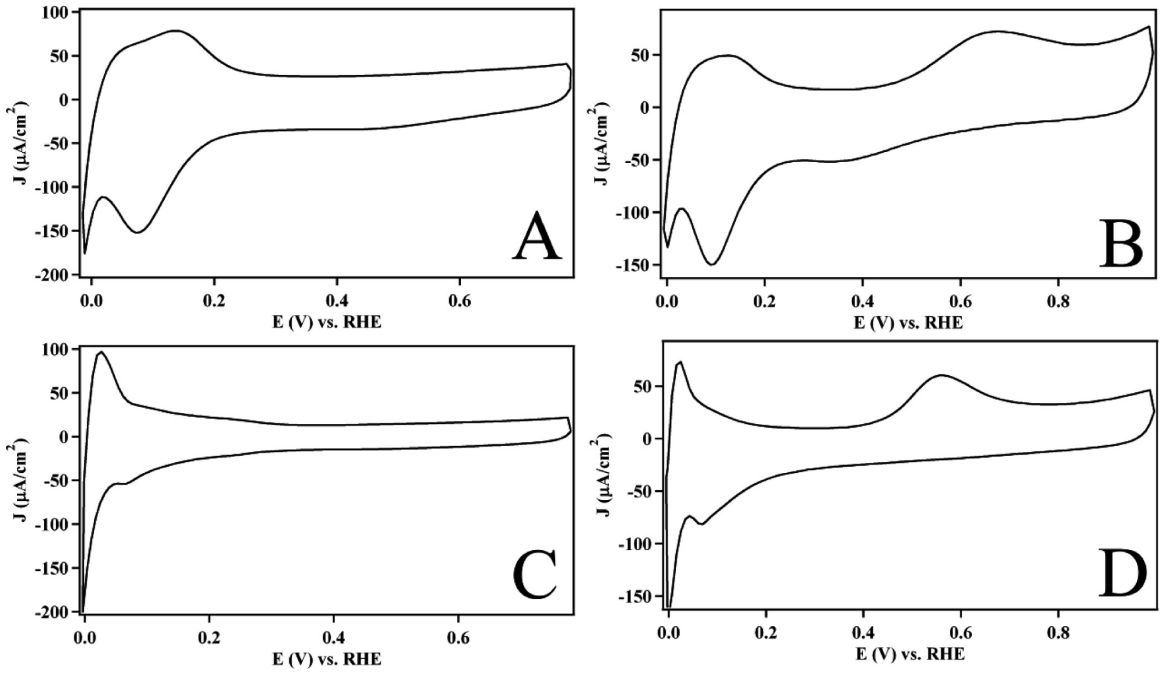

Figure 2. Representative CV curves (A and C) and CO stripping voltammograms (B and D) obtained from as-prepared Ru NWs (A and B) and commercial Ru NP/C (C and D) in 0.1 M $HClO_4$.

of amorphous RuO_2 impurities that are widely known to exist in commercial Ru NP/C catalysts.[23,27]

Several recent reports have suggested that amorphous hydrous RuO_2 retains a very high activity toward CO oxidation and that, additionally, these oxides do not undergo H_{ads}.[50] Because these oxide residues are not normally found in less oxophilic metals such as either commercial Pt or Pd NP/C, this may be a likely explanation for the distinctive behavior of Ru nanostructures. Typically, these oxide impurities in commercial Ru NP/C samples can only be selectively removed by rigorous pretreatments, such as thermal reduction under a reducing atmosphere, which is not only time-consuming and inefficient but also not amenable to scalable production.[23,27] An alternate but less likely explanation for the improved CO stripping kinetics may be the higher defect site density present on 0D nanostructures as compared with 1D nanostructures, which may serve as active sites for CO oxidation.[13,51,52] However, the presence of unique defect sites is less likely, because no characteristic features associated with defect sites are present in the so-called "preignition" region of the CO stripping CV curve.[40] Regardless of the origin of this enhancement, we have demonstrated herein that the as-received commercial Ru NP/C samples maintain improved CO stripping performance as compared with elemental NWs and that this is beneficial in terms of MOR electrocatalysis.

3.3. Morphology-Dependent Structure in Pt~Ru NWs and Pt~Ru NP/C Core−Shell Structures Prepared by Cu UPD/GD. After characterizing the structure and electrochemical properties of the Ru nanostructures, we have synthesized the desired Pt-modified Ru nanostructures (i.e., Pt~Ru NWs and Pt~Ru NP/C) utilizing a two-step protocol widely employed for the deposition of Pt atoms in monolayer-level quantities. In short, UPD is employed to deposit a monolayer quantity of Cu atoms onto the surface of the nanostructures, and these ad-atoms are subsequently displaced by immersing the Cu-modified electrode into a Pt precursor solution. In prior reports, we have successfully utilized this approach to deposit contiguous, homogeneous monolayers of Pt atoms onto the surfaces of Pd and $Pd_{1-x}Au_x$ NWs for enhanced performance toward ORR.[31,35−38] However, a rational examination of the Cu UPD/GD process on bulk Ru single crystals has revealed that the resulting Pt layer is not really homogeneous but rather consists of discrete Pt NP islands, dispersed over the single-crystal surface.[47,48]

In this report, we undertake for the first time a systematic investigation of the morphology-dependent structure of Pt layers deposited onto nanostructured Ru NWs and Ru NP/C systems, utilizing the UPD/GD protocol. In prior work, Adzic and co-workers used the UPD/GD procedure to deposit Pt onto the surface of Ru NP/C.[23,27] Optimization of the Pt content revealed that the best MOR performance was achieved when the Pt content was effectively equivalent to the quantity required for one monolayer. However, a thorough investigation of the surface and interfacial structure of these core−shell catalysts as a function of the morphology of the Ru core and the amount of Pt deposited has yet to be performed.

Herein, we have utilized HRTEM, HAADF, and EDAX to examine the structure of the Pt shell−Ru core interface as well as the Pt distribution on commercial Ru NP/C and on Ru NWs, after initiating one UPD/GD protocol. Parts A and B of Figure 3 depict overviews of HRTEM and HAADF images of Pt-decorated Ru NP/C (Pt~Ru NP/C) collected after one such UPD/GD procedure, followed by electrochemical characterization. We note that the individual particles maintain a diameter of 1.9 ± 0.5 nm and are dispersed as clusters onto the surfaces of the C support. The interplanar spacing is 0.226 ± 0.008 nm, which is measurably smaller than the corresponding value for elemental Ru (0.234 nm). A decrease in the lattice spacing suggests that Pt not only is deposited on the surface but also has been incorporated into the Ru as a genuine alloy, a scenario that had not been previously observed in the deposition of Pt on Ru NPs by a UPD/GD cycle.

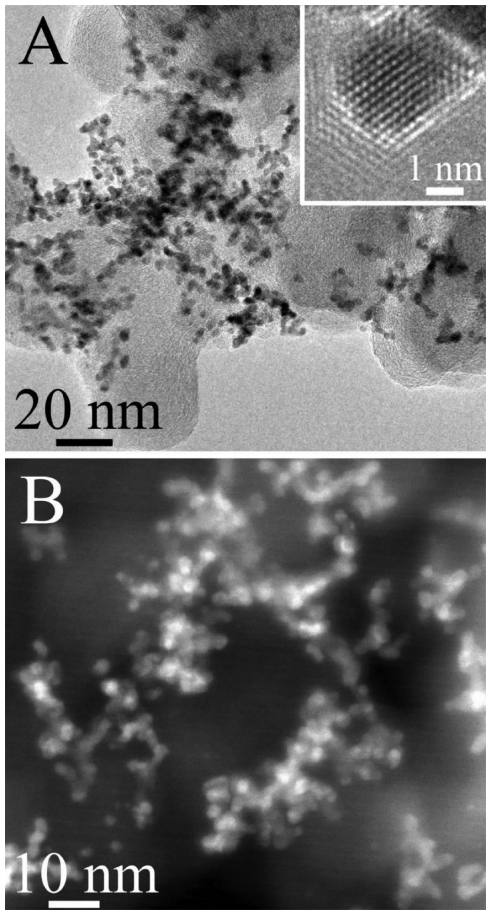

Figure 3. Representative TEM (A) and corresponding HAADF (B) images of Ru NP/C, modified with a one-monolayer quantity of Pt, utilizing a single Cu UPD/GD deposition step. A typical HRTEM image of a single, individual particle is shown as an inset.

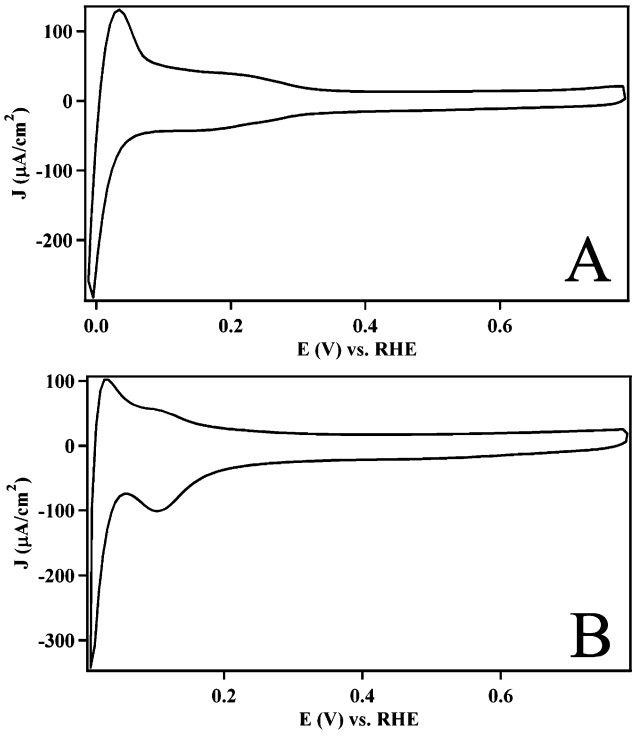

Figure 4. CV data obtained from Ru NP/C (A) and Ru NW (B), after modification with a one-monolayer quantity of Pt, utilizing a single Cu UPD/GD deposition step.

The CV data obtained from the Pt~Ru NP/C prepared by one combined UPD/GD procedure (Figure 4A) support the HRTEM analysis and indicate that an alloy-type particle is likely formed. For example, the CV curve of the Pt~Ru NP/C maintains a broad featureless H_{ads} region (i.e., 0−0.35 V) with nearly equivalent hydrogen adsorption and desorption charges. This is distinctive from analogous data from elemental Ru NP/C, which possessed a significantly larger cathodic charge associated with the combined hydrogen adsorption/oxide reduction processes. In addition, the Pt~Ru NP/C do not maintain the broad reduction feature noted in the elemental Ru NP/C, normally associated with the reduction of adsorbed surface oxide species (i.e., $Ru-O_{ads}$ to $Ru-OH_{ads}$). Collectively, these results are not consistent with the presence of Pt islands simply decorating the surface of the underlying Ru NP/C substrate, because the exposed Ru NP/C substrate would impart features in the CV similar to those observed in the CV obtained from elemental Ru NP/C (Figure 2C). Indeed, the features in the CV obtained from the Pt~Ru NP/C are analogous to those of commercial alloy-type C-supported $Pt_{1-x}Ru_x$ NPs, such as PtRu NP/C, shown in Figure S3 in the SI. In effect, these CV data in combination with the HRTEM results indicate that the surface structure of our NPs is likely analogous to an alloy-type surface structure with a homogeneous distribution of the Pt and Ru atoms at the surface as opposed to the formation of either a contiguous Pt monolayer or Pt islands, for instance. In fact, it requires up to three Cu UPD/GD cycles to create a truly uniform Pt coating on commercial Ru NP/C, on the basis of CV curves and HRTEM results.[27]

In terms of the overall homogeneity in the Pt~Ru NP/C sample, the HAADF image highlights collections of particles as well as individual particles with higher contrast than other representative regions. Because the contrast in HAADF is sensitive to the atomic number (Z), it is evident that the distribution of Pt throughout the sample is not homogeneous. To quantitatively confirm this, we obtained EDAX spectra from a variety of individual particles, and the relative atomic percentages of Pt were found to vary from 50% to as high as 90% in the regions of high contrast in the HAADF image. Although additional experiments are in progress to examine the origin of the Pt dispersion throughout the sample, this observation may likely be attributed to the high degree of aggregation and the presence of residual oxide impurities, which are intrinsic to commercial Ru NP/C samples. In essence, the presence of aggregation as well as of residual oxide impurities may render some areas of the sample electrochemically inaccessible to the UPD of Cu and the corresponding deposition of Pt by GD of the Cu.

By contrast with the Pt~Ru NP/C, a similar characterization of the Pt-decorated Ru NWs (Pt~Ru NWs) by a UPD/GD cycle highlighted in Figures 5 and S4A in the SI reveals that the Pt coalesces into complex 3D NP clusters on the Ru NW surface. It is evident from the overview TEM images in Figure 5A that the Ru NWs are decorated with spherical NPs (with an average diameter of ~30 nm), distributed over the NW surface. The higher contrast of these particles in the TEM (Figure 5A) and HAADF images (Figure 5B) suggests that they are composed primarily of Pt. The localization of Pt in the particles

dx.doi.org/10.1021/am4007462 | ACS Appl. Mater. Interfaces 2013, 5, 5518−5530

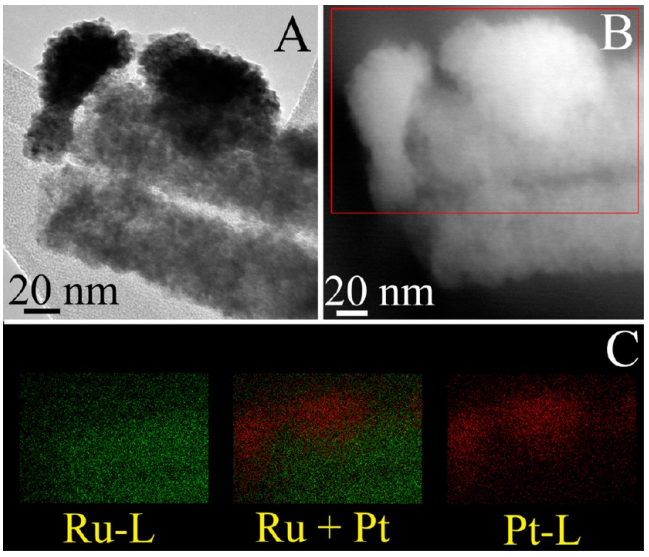

Figure 5. Characterization of Pt-modified Ru NWs after one UPD/GD cycle. TEM (A) and an HAADF (B) images of a representative Pt NP on the surface of the Ru NW. Spatially resolved EDAX maps (C), highlighting the Ru L-edge signal (left) and the Pt L-edge signal (right), along with the composite image (center).

is also evident in the spatially resolved EDAX maps (Figure 5C), which suggest that the Pt signal is concentrated in the particles along with minimal Ru signal. In fact, EDAX spectra (Figure S5 in the SI) obtained from the NP imply that the particle primarily consists of 80% Pt and only 20% Ru, while spectra obtained from the Ru NW near the position of the cluster are characterized by 80% Ru and only 20% Pt. Regions of the NW that are not exposed to the Pt cluster maintain almost 100% Ru signal, suggesting that the Pt content is highly localized in the clusters themselves.

Not surprisingly, the CV data confirm that the structure consists of discrete Pt domains present on the surface of the Ru NWs. By contrast with the Pt~Ru NP/C system, the measured charge of the feature associated with the adsorption of hydrogen in Pt~Ru NWs in the range of 0−0.2 V is considerably larger than the corresponding hydrogen desorption feature. The broad reduction feature between 0.35 and 0.7 V is also present in the CV curves of the Pt~Ru NWs. Collectively, these results are consistent with features observed from the Ru NW and indicate that the underlying Ru NW substrate is likely exposed to a measurable extent in the case of the Pt~Ru NWs; this geometric configuration is distinctive from the analogous scenario associated with Pt~Ru NP/C.

In addition, careful inspection of the CV obtained from the Pt~Ru NW (Figure 4A) also confirms that Pt is deposited and is electrochemically active on the surface. Prior results on Ru single crystals have revealed that the deposition of Pt islands on the surfaces of the underlying Ru substrate promotes the H_{ads} process and results in a significant decrease in hysteresis between the peak potentials for hydrogen adsorption (cathodic peak) and desorption (anodic peak).[47,48] This phenomenon is evident herein because we have observed a relatively small difference in potential of ~6 mV between the hydrogen adsorption and desorption peaks in the Pt~Ru NWs, which is considerably lower than that of the corresponding hysteresis in the Ru NWs (i.e., ~63 mV) before the UPD/GD process. In all, these results strongly suggest that the Pt deposited onto the NW surface coalesces into essentially clusters of elemental Pt NPs, present on the surfaces of the Ru NWs, and that significant areas of the Ru NWs, nonetheless, are still electrochemically accessible after the deposition process.

This unique 3D structure resulting from Cu UPD/GD of Pt~Ru NWs is distinctive from analogous results obtained on the Pt~Ru NP/C and raises several questions, regarding the morphology-dependent deposition of Pt on Ru nanostructures. We believe that the morphology-dependent structure of the Pt shell emerges from the unique properties associated with the Ru NWs and Ru NPs. First, it is critical to highlight that the potential window for the UPD of Cu coincides with the reduction of the adsorbed oxide species present on the Ru nanostructures, a fact that is evident in Figure S6A in the SI. Not surprisingly, parts A and C of Figure 2 demonstrate that the Ru NWs and Ru NP/C maintain very distinctive and unique surface oxide reduction profiles. Therefore, it is no wonder that the structure of the resulting Pt monolayer formed by the direct GD of the Cu layer depends upon the underlying morphology. However, the rational exploration of the UPD/GD process in this case is problematic, because the as-deposited Cu monolayer is highly sensitive to oxygen and moisture, thereby making direct examination of the Cu monolayer alone somewhat challenging.[44] In addition, the GD process occurs instantaneously, thereby rendering it difficult to observe the formation of the Pt monolayer itself. However, we were able to examine the morphology of the deposited Pt layer on these different nanostructures, utilizing a suite of electrochemical techniques, including both CV and the Cu UPD profiles themselves.

In the case of the Ru NWs, the Cu UPD profiles (Figure S6B in the SI) for the Pt~Ru NWs demonstrate a significant and measurable shift in the stripping peak of the Cu monolayer to higher potentials by comparison with the Ru NP/C. This measured shift in the stripping peak indicates that the Ru NWs maintain a stronger overall interaction with the Cu ad-atoms by comparison with the Ru NPs. Moreover, the stripping peak of the Ru NWs is broader than that of the particles, potentially resulting from the presence of a larger ensemble of active sites at the surface. Consequently, we believe that the UPD process on the larger and potentially more stable Ru NWs likely generates small islands of Pt on the surface of Ru in an analogous manner to that of bulk electrodes and single crystals. This interpretation is consistent with the observed UPD profile, particularly when compared with the potential window noted for bulk Ru electrodes.[47,48] It is conceivable that, after the UPD/GD process is complete, the as-formed islands coalesce, fuse, and aggregate upon electrochemical cycling, so as to minimize the surface energy of the system and form the apparently larger NPs, present on the surfaces of the Ru NWs.

On the other hand, the UPD profile of the Ru NP/C catalysts is distinctive from that of the Ru NWs. Specifically, it is apparent that the onset of UPD in the cathodic sweep is shifted to considerably lower potentials by comparison with the analogous Ru NWs, which likely results from the stronger interactions of the Ru NP/C with the adsorbed oxygen, evident in the CV results (Figure 2A and 2C). Although this result highlights the uniqueness of the UPD profile attributed to the Ru NP/C, it is not easy to directly correlate this observation with the formation of the alloy-type particle upon immersion in the Pt precursor solution. However, noble-metal NPs tend to be associated with higher defect site densities, and are inherently more reactive as compared with NWs, which may

thereby facilitate the reconfiguration of the surface and the corresponding formation of an alloy-type structure.[32]

Although we have provided a useful means for understanding the origin of the noticeably different deposition behavior of Pt on Ru NWs versus Ru NP/C, it is evident that further work beyond the scope of this report is necessary to develop a better understanding of the UPD/GD process on Ru. However, it is critical to highlight that this unique morphology-dependent process governs the formation of robust Ru-based core−shell structures.

3.4. Optimization of Electrocatalytic Activity and Performance of Core−Shell Pt~Ru NWs and Pt~Ru NPs in Relation to Commercial Pt NP/C and PtRu NP/C Standards. The opportunity to control the structure of the Pt−Ru interface as a function of the catalyst morphology is an important element in moving toward rationally tuning the electrocatalytic performance of core−shell-type architectures. Herein, we investigate the MOR performance of as-prepared Pt~Ru NWs and Pt~Ru NPs, which includes assessing both the activity of as-prepared catalysts and their durability. Initially, we examined the performance of the Pt-modified Ru NWs and Ru NP/C as a function of the number of UPD/GD Pt deposition steps. In the case of Pt~Ru NP/C, the optimal MOR performance was achieved after one UPD/GD step, which is in excellent agreement with prior reports.[23] Previous results obtained from homogeneous, alloy-type commercial $Pt_{1-x}Ru_x$ NP/C have revealed that the optimal electrochemical performance is achieved between 70 and 90% Pt, which is expected to give rise to a suitable density of Pt−Ru bimetallic pair sites.[20] A high density of bimetallic pair sites at the catalytic interface may facilitate the rapid oxidation of methanol at relative low overpotentials, because the more oxophilic Ru sites can selectively oxidize the poisoning CO intermediate via the bifunctional mechanism. Thus, it is not surprising that Pt~Ru NP/C maintain an optimum performance after one UPD/GD cycle, because we have demonstrated herein that these particles possess an alloy-type structure with the Pt composition ranging from 50 to 90%. In essence, our as-synthesized Pt~Ru NPs possess an ideal surface structure and chemical composition for MOR.

A similar investigation of the MOR performance on the Ru NWs as a function of the number of UPD/GD steps reveals an interesting trend that is contrary to that observed for analogous Ru NPs. In this case, we noted a systematic volcano-type dependence of the mass- and area-normalized MOR current density as a function of the number of UPD/GD cycles (Figure S7 in the SI) with an optimal performance achievable after a total of six deposition steps. TEM images (Figure S4B in the SI) of the Ru NWs with increasing UPD/GD deposition steps highlight an increase in the density of the Pt particles, coating the surface of the Ru NWs. On this basis, it is evident that the trend of increasing specific MOR activity over the initial Pt deposition cycles arises from the addition of Pt-enriched NPs onto the surfaces of the underlying Ru NW substrate, thereby creating active Pt sites on the NPs and highly active Pt−Ru pair sites at the interface between the Pt NPs and the underlying Ru NW substrate. Inevitably, further deposition steps will fully cover the underlying Ru substrate, thereby reducing the number of Pt−Ru pair sites and ultimately resulting in the net formation of a surface looking more like elemental Pt. This situation would coincide with the sharp decrease in the specific activity, observed after six UPD/GD cycles.

Careful inspection of the area-normalized LSVs (Figure S7A in the SI) provides evidence for this phenomenon, because the MOR curve shifts to higher potentials as the number of deposition cycles approaches seven. This indicates that there is a lower overall CO tolerance, coinciding with the presence of fewer bimetallic pair sites, as the surface becomes fully covered by the Pt. To systematically validate the idea of six UPD/GD cycles as providing for an optimum Pt coverage, we have utilized a high-throughput deposition method in order to prepare several different Pt~Ru NW samples with six UPD/GD deposition cycles, and we have observed consistent and reasonable area- and mass-normalized peak activities of 1.8 ± 0.2 mA/cm^2 and 2.3 ± 0.3 A/mg, respectively.

Once the Pt loading was examined and optimized, the activity and durability of the Pt~Ru NW (i.e., six UPD/GD cycles) and Pt~Ru NP (i.e., one UPD/GD cycle) electrocatalysts were studied by comparison with Pt NP/C and homogeneous alloy-type PtRu NP/C, mutually serving as state-of-the-art commercial standards. The ESA-normalized LSVs in Figure 6A highlight a prominent oxidation peak associated with

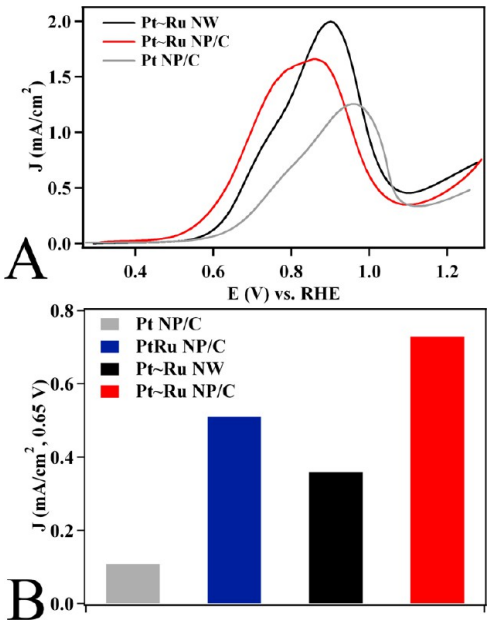

Figure 6. Area-normalized LSVs obtained in 0.5 M methanol in a 0.1 M $HClO_4$ supporting electrolyte at 20 mV/s. The specific activities of the various electrocatalysts, including those of commercial Pt NP/C and alloy-type PtRu NP/C, as well as our optimized Pt~Ru NP/C (i.e., one UPD/GD cycle) and Pt~Ru NWs (i.e., six UPD/GD cycles), were measured at 0.65 V.

the electrocatalytic oxidation of methanol. To quantitatively evaluate the various intrinsic activities of the different catalysts toward MOR, we compared the current density of each catalyst measured at 0.65 V (Figure 6B), which serves as a reasonable potential in the onset region of the LSV curve. We specifically elected to utilize the LSV of Pt NP/C so as to highlight the specific effects of a Ru substrate upon the Pt active sites in the case of the Pt~Ru NWs and Pt~Ru NP/C because Pt NP/C represents a commercial catalyst containing solely Pt active sites. The measured current at 0.65 V can then be subsequently normalized to either the catalyst surface area, thereby providing for an area-normalized "specific activity", or to the mass of the

dx.doi.org/10.1021/am4007462 | ACS Appl. Mater. Interfaces 2013, 5, 5518−5530

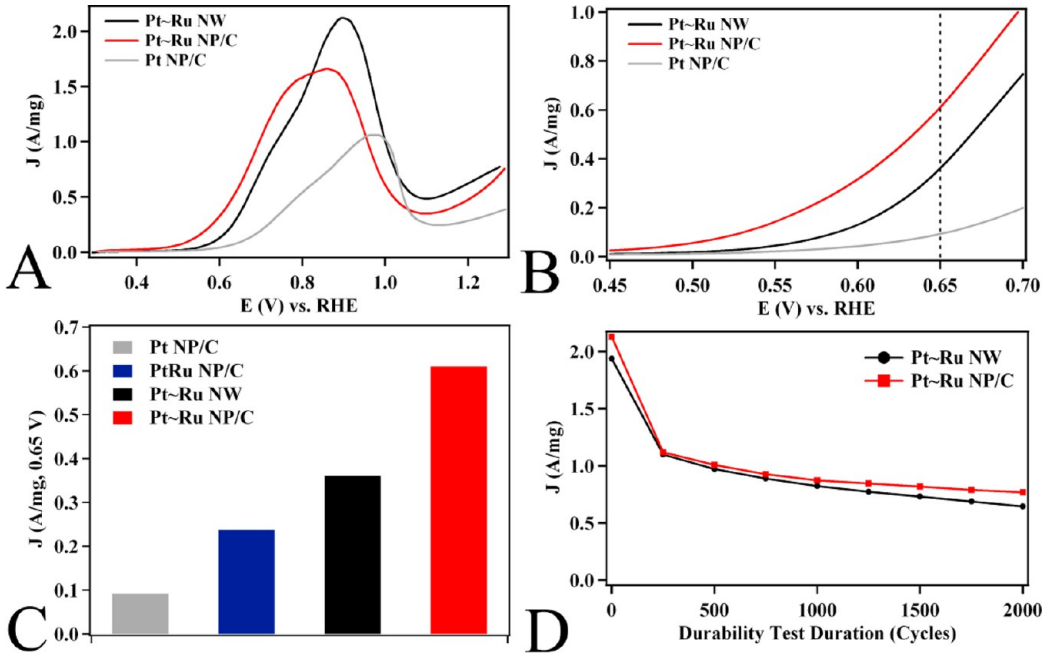

Figure 7. Mass-normalized LSVs (A) obtained in 0.5 M methanol in 0.1 M $HClO_4$ at 20 mV/s with the onset region for MOR highlighted (B). The mass activities measured at 0.65 V (C) are shown for the commercial Pt NP/C and PtRu NP/C and for our corresponding as-prepared core−shell Pt~Ru NP/C (i.e., one UPD/GD cycle) and Pt~Ru NW (i.e., six UPD/GD cycles) electrocatalysts. A plot of the mass-normalized current density at 0.64 V as a function of the cycle number in a durability test (D) is also shown.

Pt present within the same catalyst, yielding the analogous "mass activity".

Using the specific activity as a measure of the intrinsic catalyst performance, we first compared the performance of Pt~Ru NWs with that of elemental Pt NP/C and homogeneous, alloy-type PtRu NP/C in order to examine their performance in the context of state-of-the-art commercial catalysts, possessing Pt active sites and Pt−Ru active sites, respectively. The optimized Pt~Ru NWs displayed a specific activity of 0.36 mA/cm^2, which represents a considerable enhancement of over 3-fold as compared with commercial Pt NP/C (0.11 mA/cm^2). In addition, it is also evident in the onset region of the LSV, which shows that the Pt~Ru NWs maintain a measurably lower onset potential or so-called "overpotential" as compared with Pt NP/C. These data are not surprising because, as we have seen, the structures of the Pt~Ru NWs possess bimetallic Pt−Ru pair sites, localized at the interface between the Pt NP shell and the Ru NW core. The presence of these pair sites, observable in the structural and electrochemical characterization of the Pt~Ru NWs, should render them more active toward MOR as compared with the elemental Pt NP/C, because they can facilitate oxidation of the CO intermediate.[10,53,54]

However, we found that the specific activity of the Pt~Ru NWs does not exceed the corresponding specific activity of the alloy-type PtRu NP/C (0.51 mA/cm^2). Because the commercial alloy-type PtRu NP/C are characterized by a high density of well-ordered Pt−Ru pair sites, the above observations suggest that the Pt~Ru NWs do not maintain the same degree of well-ordered bimetallic pair sites as that of the corresponding alloy-type PtRu NP/C or, more importantly, Pt~Ru NP/C. Indeed, the higher intrinsic activity of the PtRu NP/C may also arise from beneficial electronic factors inherent to their alloy-type structure, which further improves upon their CO tolerance.[55] Because our HRTEM, EDAX, and CV results confirm that the Pt~Ru NWs do not undergo significant alloying of the Pt and Ru components, we postulate that the Pt~Ru NWs likely do not maintain significant enhancement in performance, essentially because of electronic and structural effects.

In a more practical sense, we can also compare the performance of the Pt~Ru NWs with that of the state-of-the-art commercial standards in the context of their activity, normalized to the Pt mass present. The high Pt loading requirement inherent to DMFCs continues to be a critical challenge in their practical development, because of Pt's high cost and relatively low abundance. Hence, to quantitatively investigate the intrinsic activity associated with the Pt content of the catalysts, the MOR LSVs (Figure 7A,B) can be normalized to the Pt content of the catalyst, so as to provide for a mass-normalized activity. The Pt mass activity (Figure 7C) of the Pt~Ru NWs was determined to be 0.36 A/mg, which was considerably higher than the corresponding activities for the commercial Pt NP/C (0.092 A/mg) and alloy-type PtRu NP/C (0.237 A/mg), respectively. The increased mass activity in the Pt~Ru NWs emphasizes the distinctive advantages of the core−shell architecture, because all of the Pt content is effectively localized at the catalytic interface. Consequently, this geometry results in a relatively higher Pt mass activity for the Pt~Ru NWs, despite their lower specific activity as compared with the alloy-type PtRu NP/C system.

In addition, we can also examine the performance of the optimized Pt~Ru NP/C catalyst with respect to state-of-the-art commercial standards. The Pt~Ru NPs (0.73 mA/cm^2) possess a 1.5-fold higher specific activity than the corresponding commercial alloy-type PtRu NP/C. This result is in excellent agreement with our HRTEM and EDAX data, which revealed that the Pt~Ru NPs comprise a structure that is analogous to an alloy-type configuration with an average chemical composition of 70% Pt. The higher Pt content in the Pt~Ru

dx.doi.org/10.1021/am4007462 | ACS Appl. Mater. Interfaces 2013, 5, 5518−5530

NPs (70%) as compared with that found in alloy-type PtRu NP/C (50%) readily explains their higher activity toward MOR.[56] In fact, similar enhancements in the mass activity (0.61 A/mg) have also been noted in Pt~Ru NPs, which are as much as 6-fold and 3-fold higher compared with commercial Pt NP/C and PtRu NP/C, respectively. Overall, these data are consistent with the very reasonable notion of a higher intrinsic activity due to the spatial localization of the Pt content on the surfaces of the Pt~Ru NP/C catalysts.

3.5. Morphology-Dependent Electrocatalytic Activity and Durability in Pt~Ru NW Core−Shell Nanostructures. With an understanding of the performance of novel Pt~Ru NWs and Pt~Ru NP/C core−shell catalysts in the context of commercial catalysts, we subsequently examined the morphology-dependent performance in intrinsic activity by comparing the optimized Pt~Ru NWs (i.e., six UPD/GD cycles) with the optimized Pt~Ru NP/C (i.e., one UPD/GD cycle). The measured specific activity of the Pt~Ru NP/C (0.73 mA/cm^2) was found to be 2-fold higher than that of the Pt~Ru NWs (0.36 mA/cm^2) when measured at 0.65 V. The onset potential of the MOR current density is also considerably lower by ~100 mV, suggesting that the Pt~Ru NPs are intrinsically more active than the Pt~Ru NWs.

On the basis of our comparison of these catalysts with the corresponding Pt NP/C and alloy-type PtRu NP/C commercial standards, the enhanced initial performance of the Pt~Ru NP/C can be readily attributed to the formation of an alloy-type surface structure, which is distinctive from the hierarchical structure formed in the analogous Pt~Ru NWs. Specifically, the Pt~Ru NP/C can possess an optimal composition regime and a high density of bimetallic pair sites for efficient MOR catalysis, which would impart both improved MOR kinetics and a lower onset potential. On the other hand, the Pt~Ru NWs maintain the presence of nearly pure Pt clusters on their external surface, wherein bimetallic sites can only be present at the interface between the clusters and the Ru NW itself. In terms of the mass activity, the pristine and optimized Pt~Ru NP (0.61 A/mg) catalysts consistently outperform the analogous Pt~Ru NWs (0.36 A/mg) by nearly 2-fold, which makes sense in the context of the idea of the area-normalized performance.

Although these results would potentially point toward the Ru NPs as an optimized morphology for Pt deposition and MOR electrocatalysis, we have rationally investigated the performance of the Pt~Ru NW and Pt~Ru NP catalysts in a simulated durability test. Durability tests are a crucial step for evaluating the potential of catalyst systems for long-term use in practical fuel-cell systems. The durability test utilized herein consists of a rigorous protocol, wherein the electrode is repeatedly cycled in a 0.5 M methanol solution (0.1 M $HClO_4$), and the mass activity is monitored over the course of 2000 electrochemical cycles.

The results of this test (Figure 7D) revealed that the high initial activity of both the Pt~Ru NWs and Pt~Ru NPs quickly declines within the first 250 cycles, and from 250 to 2000 cycles, a slow decline is noted in both systems. Surprisingly, the Pt~Ru NP/C and Pt~Ru NWs maintain essentially identical mass-normalized activities of ~1.0 A/mg after the first 250 cycles. This is significant because the initial 2-fold enhancement in the activity of the Pt~Ru NP/C with respect to the Pt~Ru NWs is reduced to practically identical performance. In the subsequent 250−2000 cycles, the activities of both catalysts undergo slight declines, and at the conclusion of the durability test, the Pt~Ru NP/C system retains only a marginal improvement of 15%. In essence, both catalysts evince essentially a similar performance, despite the initial 2-fold enhancement observed in the Pt~Ru NP/C with respect to the Pt~Ru NWs. These findings from the durability test conclusively demonstrate that the unique structure and morphology of the deposited Pt promotes a trade-off between the higher initial activity of the alloy-type structure in the Pt~Ru NP/C and the greater structural stability of the Pt~Ru NWs, which collectively "balance out" to yield comparable performances in MOR electrocatalytic behavior after 2000 cycles.

In the case of small NPs, we have demonstrated that deposition of Pt onto commercial Ru NP/C (Pt~Ru NP/C) results in an alloy-type surface structure, which maintains a high density of pair sites and is optimal for MOR performance. In terms of catalytic advantages, the alloy-type structure adopted by the Pt~Ru NP/C promotes increased MOR activity by nearly 2-fold in the initial cycles. However, the Pt~Ru NP/C system undergoes significant particle ripening, which is accompanied by a lower dispersion of the catalyst onto the C support surface. The problem of catalyst ripening in particles with small diameters has been commonly observed, and represents a key challenge in their development as practical electrocatalysts.[15] Because the alloy-type chemical structure is expected to impart a high tolerance to poisoning intermediates, we believe that the significant activity loss in the first 250 cycles can be attributed to the observed structural reconfiguration, thereby resulting in a loss of effective catalyst's ESA and a corresponding decrease in the mass-normalized performance.

In the case of the Pt~Ru NWs, we have demonstrated that larger Ru NWs form a 3D structure, consisting of nearly pure Pt clusters, which possess pair sites only at the physical interface between the cluster and the underlying Ru NW substrate. Accordingly, we have also shown that the initial activity of the Pt~Ru NWs is lower than that of the Pt~Ru NP/C. However, the real advantage of the Pt~Ru NWs becomes apparent during the durability testing, and after 250 cycles, the Pt~Ru NWs and Pt~Ru NP/C maintain essentially the same mass activity of ~1 A/mg. At the conclusion of the test, the activities of the Pt~Ru NP/C and Pt~Ru NWs give rise to a performance nearly identical with that of the activity of the Pt~Ru NP/C, which is only 15% higher than the corresponding Pt~Ru NWs. This result raises an important question regarding the performance of these catalysts. Specifically, why is the initial enhancement in the activity of the Pt~Ru NP/C not conserved over the duration of the durability test?

Therefore, to account for this apparent discrepancy, the morphology of the Pt~Ru NWs was investigated after 2000 cycles of a rigorous durability test, and a representative TEM image is shown in Figure S8 in the SI. It is apparent that the structural integrity of the hierarchical structure, consisting of the Pt clusters deposited on the surface of the Ru NW, is largely maintained, even after the testing. In fact, measurements of the Pt clusters confirm that the average diameter does not significantly change from the diameters measured prior to the durability test. Additionally, the Ru NW substrates retain their distinctive 1D morphology. However, the evolution of some porosity in the Ru NWs is evident. This is not surprising and has been previously observed and studied in analogously synthesized Pd NWs, after characterization of their durability for ORR.[36,38] In fact, prior results by our group have revealed that noble metal NWs possess significantly better structural

durability as a result of their anisotropic structure, which has been shown to reduce both oxidation and ripening processes.[31,35,36,39]

From these results, it is clear that the 1D hierarchical structure of the Pt~Ru NWs does not suffer from either significant particle ripening, dissolution, or aggregation and that this structural motif represents a distinctive advantage over that of Pt~Ru NP/C. Because the loss in activity over the first 250 cycles does not occur from significant structural reconfiguration, we can attribute the observed activity loss to the effects of poisoning from the formation of partially oxidized carbon intermediates. Although the Pt~Ru NWs maintain Pt−Ru pair sites at the cluster−NW interface, the essentially elemental Pt clusters are expected to be more susceptible to poisoning, especially as compared with the Pt~Ru NP/C, thereby explaining the observed activity decline. However, it is apparent that the significant structural changes observed in the Pt~Ru NP/C lead to a proportionally higher loss in activity, particularly as compared with the poisoning effects associated with the Pt~Ru NWs. Thus, the comparable activity observed in the Pt~Ru NP/C and Pt~Ru NWs at the conclusion of the durability test can be reasonably rationalized in the context of all of these data.

Collectively, the structure and morphology-dependent performance observed herein is a significant result and represents a critical advance toward understanding the electrocatalytic performance of these novel core−shell-type Pt~Ru nanostructures. First, we demonstrate that the deposition of Pt by Cu UPD onto an underlying Ru substrate is a complex and sensitive process, which does not necessarily lead to the formation of uniform Pt monolayers, as is the case with other noble metal nanostructures. Nevertheless, the importance of using hierarchical structures, particularly those possessing 1D structures, for key electrochemical reactions has recently been highlighted, because of their unique structure and corresponding ability to tailor the catalytic interface. Specifically, this potential capability can be achieved by rationally modifying elements of this architecture, such as either the density of the clusters or their size.[57,58]

In our particular experiments, the Pt~Ru NWs represent a key platform in terms of developing highly effective ORR electrocatalysts that are also tolerant to the presence of small organic molecules, such as methanol. The problem of methanol crossover in DMFCs continues to be a critical technological hurdle in their practical development and, as such, necessitates innovation at many levels.[59] In the Pt~Ru NW architecture, in particular, the highly active elemental Pt clusters are anticipated to be active ORR catalysts. Additionally, the Pt−Ru pair sites present at the interface may serve as catalysts for the removal of CO that is generated during the ORR in the presence of methanol. Although it is beyond the scope of this report, experiments are currently under way to characterize the ORR activity and corresponding durability of these hierarchical structures.

Overall, the results herein imply the creation of a useful nanoscale platform and an excellent model system for investigating the structure and morphology of the interface between the Pt "shell" and the underlying Ru "core" after deposition, a feat that should enable further optimization of the density, location, and uniformity of bimetallic Pt−Ru pair sites for yielding enhanced performance in MOR. All of these findings represent a positive advance toward understanding the structure and reactivity of core−shell Pt~Ru structures for practical applications.

4. CONCLUSIONS

Elemental Ru gives rise to promising applications in a variety of emerging technologies, and there is a growing need for reliable synthetic techniques for the production of nanostructured Ru with control over their size, shape, and morphology. Herein, we report for the first time a simple, ambient approach for the synthesis of crystalline Ru NWs that relies on a proven template-based method. This facile protocol represents a significant advance, because we can prepare NWs with diameter control under ambient, surfactantless, catalyst-free conditions, without the need for either acidic electrolytes or any additional experimental equipment. The Ru NWs themselves maintain a high degree of purity and crystallinity, and possess electrochemical properties that are consistent with elemental Ru itself.

Drawing upon the idea of structure−property correlations in these anisotropic nanostructures, we have investigated their morphology-dependent electrocatalytic performance toward methanol oxidation for these Pt-modified Ru nanostructured catalysts. The deposition of Pt has been accomplished by a two-step UPD/GD process, and the resulting core−shell architectures displayed significant morphology dependence with respect to the structure of the Pt−Ru interface. The specific MOR activity highlights the distinctive structure of the Pt−Ru interface after Pt deposition. Indeed, the data reveal that the Pt~Ru NPs form an alloy-type structure, whereas the Pt~Ru NWs consist of a Pt NP shell affixed to the Ru NW core. The alloy-type structure of the commercial Pt~Ru NPs promotes significantly enhanced specific and mass-normalized MOR activity as a result of the high density of Pt−Ru pair sites.

The long-term durability testing data demonstrate that the Pt~Ru NWs and Pt~Ru NP/C maintain distinctive advantages in the role of MOR catalysts. Specifically, the alloy-type structure of the Pt~Ru NP/C promotes high activity in the initial cycles. However, during cycling, the effects of particle aggregation and ripening may result in significant declines in performance. On the other hand, the anisotropic nature of the Pt~Ru NW motif renders it less susceptible toward structural reconfiguration. However, the susceptibility of the Pt clusters to poisoning can result in significant decreases in activity. After 2000 cycles, the Pt~Ru NP/C gives rise to only a slight improvement in activity over that of the corresponding Pt~Ru NWs. Collectively, these results yield important insights into the fundamental development of complex Ru-based architectures, which certainly represent a promising new structural paradigm toward advancing the commercial viability of DMFCs.

■ ASSOCIATED CONTENT

Ⓢ Supporting Information

Additional figures including structural (XRD, SEM, TEM, and EDAX) and electrochemical (CV curves and MOR LSVs) characterization. This material is available free of charge via the Internet at http://pubs.acs.org.

■ AUTHOR INFORMATION

Corresponding Author

*E-mail: stanislaus.wong@stonybrook.edu or sswong@bnl.gov.

Notes

The authors declare no competing financial interest.

■ ACKNOWLEDGMENTS

Research (including support for S.S.W. and electrochemical experiments) was supported by the U.S. Department of Energy, Basic Energy Sciences, Materials Sciences and Engineering Division. Support for experimental supplies was also provided by Sigma Xi through its Grants-in-Aid of Research Program. We acknowledge Dr. R. R. Adzic and Dr. M. B. Vukmirovic (Brookhaven National Laboratory) for relevant, helpful discussions and assistance with obtaining electrochemical measurements. We also thank Dr. J. Quinn and Dr. A. C. Santulli for their assistance with obtaining SEM and EDAX measurements. Experiments for this manuscript were performed, in part, at the Center for Functional Nanomaterials located at Brookhaven National Laboratory, which is supported by the U.S. Department of Energy under Contract DE-AC02-98CH10886.

■ REFERENCES

(1) Astruc, D.; Lu, F.; Aranzaes, J. R. *Angew. Chem., Int. Ed.* **2005**, *44*, 7852−7872.
(2) Viau, G.; Brayner, R.; Poul, L.; Chakroune, N.; Lacaze, E.; Fiévet-Vincent, F.; Fiévet, F. *Chem. Mater.* **2002**, *15*, 486−494.
(3) Campelo, J. M.; Luna, D.; Luque, R.; Marinas, J. M.; Romero, A. A. *ChemSusChem* **2009**, *2*, 18−45.
(4) Ducati, C.; Dawson, D. H.; Saffell, J. R.; Midgley, P. A. *Appl. Phys. Lett.* **2004**, *85*, 5385−5387.
(5) Gual, A.; Godard, C.; Castillón, S.; Curulla-Ferré, D.; Claver, C. *Catal. Today* **2012**, *183*, 154−171.
(6) Hennings, U.; Reimert, R. *Appl. Catal., B* **2007**, *70*, 498−508.
(7) Joo, S. H.; Park, J. Y.; Renzas, J. R.; Butcher, D. R.; Huang, W.; Somorjai, G. A. *Nano Lett.* **2010**, *10*, 2709−2713.
(8) Sutter, P. W.; Flege, J.-I.; Sutter, E. A. *Nat. Mater.* **2008**, *7*, 406−411.
(9) Aricò, A. S.; Srinivasan, S.; Antonucci, V. *Fuel Cells* **2001**, *1*, 133−161.
(10) Liu, H.; Song, C.; Zhang, L.; Zhang, J.; Wang, H.; Wilkinson, D. P. *J. Power Sources* **2006**, *155*, 95−110.
(11) Shukla, A. K.; Ravikumar, M. K.; Gandhi, K. S. *J. Solid State Electrochem.* **1998**, *2*, 117−122.
(12) Wasmus, S.; Küver, A. *J. Electroanal. Chem.* **1999**, *461*, 14−31.
(13) Maillard, F.; Eikerling, M.; Cherstiouk, O. V.; Schreier, S.; Savinova, E.; Stimming, U. *Faraday Discuss.* **2004**, *125*, 357−377.
(14) Maillard, F.; Savinova, E. R.; Stimming, U. *J. Electroanal. Chem.* **2007**, *599*, 221−232.
(15) Shao, Y.; Yin, G.; Gao, Y. *J. Power Sources* **2007**, *171*, 558−566.
(16) Wang, J. X.; Robinson, I. K.; Ocko, B. M.; Adzic, R. R. *J. Phys. Chem. B* **2004**, *109*, 24−26.
(17) Wee, J.-H.; Lee, K.-Y. *J. Power Sources* **2006**, *157*, 128−135.
(18) Hamnett, A. In *Interfacial Electrochemistry: Theory, Experiment and Applications*; Wieckowski, A., Ed.; Marcel Dekker: New York, 1999; pp 843−879.
(19) Liu, P.; Nørskov, J. K. *Fuel Cells* **2001**, *1*, 192−201.
(20) Wang, H.; Alden, L. R.; DiSalvo, F. J.; Abruña, H. c. D. *Langmuir* **2009**, *25*, 7725−7735.
(21) Christoffersen, E.; Liu, P.; Ruban, A.; Skriver, H. L.; Nørskov, J. K. *J. Catal.* **2001**, *199*, 123−131.
(22) Zhao, X.; Yin, M.; Ma, L.; Liang, L.; Liu, C.; Liao, J.; Lu, T.; Xing, W. *Energy Environ. Sci.* **2011**, *4*, 2736−2753.
(23) Sasaki, K.; Adzic, R. R. *J. Electrochem. Soc.* **2008**, *155*, B180−B186.
(24) Kuk, S. T.; Wieckowski, A. *J. Power Sources* **2005**, *141*, 1−7.
(25) Du, B.; Rabb, S. A.; Zangmeister, C.; Tong, Y. *Phys. Chem. Chem. Phys.* **2009**, *11*, 8231−8239.
(26) Chen, W.; Xu, L.-P.; Chen, S. *J. Electroanal. Chem.* **2009**, *631*, 36−42.
(27) Yang, L.; Vukmirovic, M. B.; Su, D.; Sasaki, K.; Herron, J. A.; Mavrikakis, M.; Liao, S.; Adzic, R. R. *J. Phys. Chem. C* **2012**.
(28) Huang, M.; Dong, G.; Wang, N.; Xu, J.; Guan, L. *Energy Environ. Sci.* **2011**, *4*, 4513−4516.
(29) Morozan, A.; Jousselme, B.; Palacin, S. *Energy Environ. Sci.* **2011**, *4*, 1238−1254.
(30) Antolini, E.; Perez, J. *J. Mater. Sci.* **2011**, *46*, 1−23.
(31) Koenigsmann, C.; Scofield, M. E.; Liu, H.; Wong, S. S. *J. Phys. Chem. Lett.* **2012**, *3*, 3385−3398.
(32) Koenigsmann, C.; Wong, S. S. *Energy Environ. Sci.* **2011**, *4*, 1161−1176.
(33) Patete, J. M.; Peng, X.; Koenigsmann, C.; Xu, Y.; Karn, B.; Wong, S. S. *Green Chem.* **2011**, *13*, 482−519.
(34) Tiano, A. L.; Koenigsmann, C.; Santulli, A. C.; Wong, S. S. *Chem. Commun.* **2010**, *46*, 8093−8130.
(35) Koenigsmann, C.; Santulli, A. C.; Gong, K.; Vukmirovic, M. B.; Zhou, W.-p.; Sutter, E.; Wong, S. S.; Adzic, R. R. *J. Am. Chem. Soc.* **2011**, *133*, 9783−9795.
(36) Koenigsmann, C.; Santulli, A. C.; Sutter, E.; Wong, S. S. *ACS Nano* **2011**, *5*, 7471−7487.
(37) Koenigsmann, C.; Sutter, E.; Adzic, R. R.; Wong, S. S. *J. Phys. Chem. C* **2012**, *116*, 15297−15306.
(38) Koenigsmann, C.; Sutter, E.; Chiesa, T. A.; Adzic, R. R.; Wong, S. S. *Nano Lett.* **2012**, *12*, 2013−2020.
(39) Koenigsmann, C.; Zhou, W.-p.; Adzic, R. R.; Sutter, E.; Wong, S. S. *Nano Lett.* **2010**, *10*, 2806−2811.
(40) Zhou, W.-p.; Li, M.; Koenigsmann, C.; Ma, C.; Wong, S. S.; Adzic, R. R. *Electrochim. Acta* **2011**, *56*, 9824−9830.
(41) Zhou, H.; Zhou, W.-p.; Adzic, R. R.; Wong, S. S. *J. Phys. Chem. C* **2009**, *113*, 5460−5466.
(42) Ponrouch, A.; Garbarino, S.; Pronovost, S.; Taberna, P.-L.; Simon, P.; Guay, D. *J. Electrochem. Soc.* **2010**, *157*, K59−K65.
(43) Zhang, F.; Wong, S. S. *ACS Nano* **2009**, *4*, 99−112.
(44) Vukmirovic, M. B.; Bliznakov, S. T.; Sasaki, K.; Wang, J. X.; Adzic, R. R. *Electrochem. Soc. Interface* **2011**, *20*, 33−40.
(45) Garsany, Y.; Baturina, O. A.; Swider-Lyons, K. E.; Kocha, S. S. *Anal. Chem.* **2010**, *82*, 6321−6328.
(46) Nagel, T.; Bogolowski, N.; Baltruschat, H. *J. Appl. Electrochem.* **2006**, *36*, 1297−1306.
(47) Hoster, H.; Richter, B.; Behm, R. J. *J. Phys. Chem. B* **2004**, *108*, 14780−14788.
(48) Hoster, H. E.; Janik, M. J.; Neurock, M.; Behm, R. J. *Phys. Chem. Chem. Phys.* **2010**, *12*, 10388−10397.
(49) Marinkovic, N. S.; Vukmirovic, M. B.; Adzic, R. R. In *Modern Aspects of Electrochemistry*; Vayenas, C., Ed.; Springer: New York, 2008; Vol. *42*.
(50) Rolison, D. R.; Hagans, P. L.; Swider, K. E.; Long, J. W. *Langmuir* **1999**, *15*, 774−779.
(51) Tsou, Y. M.; Cao, L.; Castro, E. D. *ECS Trans.* **2008**, *13*, 67−84.
(52) Vidakovic, T.; Christov, M.; Sundmacher, K. *Electrochim. Acta* **2007**, *52*, 5606−5613.
(53) Feibelman, P. J.; Hammer, B.; Nørskov, J. K.; Wagner, F.; Scheffler, M.; Stumpf, R.; Watwe, R.; Dumesic, J. *J. Phys. Chem. B* **2000**, *105*, 4018−4025.
(54) Liu, P.; Logadottir, A.; Nørskov, J. K. *Electrochim. Acta* **2003**, *48*, 3731−3742.
(55) Strasser, P.; Fan, Q.; Devenney, M.; Weinberg, W. H.; Liu, P.; Nørskov, J. K. *J. Phys. Chem. B* **2003**, *107*, 11013−11021.
(56) Basnayake, R.; Li, Z.; Katar, S.; Zhou, W.; Rivera, H.; Smotkin, E. S.; Casadonte, D. J.; Korzeniewski, C. *Langmuir* **2006**, *22*, 10446−10450.
(57) Lim, B.; Jiang, M.; Camargo, P. H. C.; Cho, E. C.; Tao, J.; Lu, X.; Zhu, Y.; Xia, Y. *Science* **2009**, *324*, 1302−1305.
(58) Tan, Y.; Fan, J.; Chen, G.; Zheng, N.; Xie, Q. *Chem. Commun.* **2011**, *47*, 11624−11626.
(59) Heinzel, A.; Barragán, V. M. *J. Power Sources* **1999**, *84*, 70−74.